3-2021

A piecewise analysis model for electrical conductivity calculation from time domain reflectometry waveforms

Zhuangji Wang
U.S. Department of Agriculture

Dennis Timlin
U.S. Department of Agriculture

Yuki Kojima
Gifu University

Chenyi Luo
Beijing University of Chinese Medicine

Yan Chen
China Agricultural University

See next page for additional authors

A piecewise analysis model for electrical conductivity calculation from time domain reflectometry waveforms

Abstract

Electrical conductivity (EC) represents a material's ability to conduct electric current. Soil EC has been used as a soil quality attribute related to soil pH, nutrient availability, crop suitability and soil microbial activity. Time domain reflectometry (TDR) estimates soil water content and EC based on the propagation/reflection and energy attenuation of voltage signals along a waveguide. To maximize the data use efficiency, waveform interpretations for simultaneous water content and EC determination are needed. A tangent line/bounded mean oscillation (TL-BMO) model is available to estimate soil water content from TDR waveforms, but an associated EC model is not yet available. The objectives of this study are (1) to introduce a piecewise analysis method for TDR waveform interpretation, and (2) to develop a model for EC computation along a TDR waveguide under homogeneous water content. The proposed model sequentially fits a TDR waveform for the coaxial cable, the connection, and the waveguide according to the transmission line equation. A TDR waveguide can be discretized into multiple successive pieces for the determination of EC variations along the waveguide. Simplifications of the fitting procedures via (1) existing models, e.g., TL-BMO and Topp et al. (1988) models, and (2) analysis of waveforms obtained from controlled conditions, e.g., in distilled water under room temperature (~20 °C) and air pressure (~101 kPa), are also applied. Accuracy and stability of the proposed model are tested via observed TDR waveforms obtained under uniform EC conditions but perturbated with a range of noise levels. EC values computed with only one discretized piece (i.e., no discretization along the waveguide) are consistent with the theoretical EC values, and the results are robust for all of the tested noise levels. As the number of discretized pieces and the noise levels increase, numerical oscillations in the results increase. The maximum relative errors are <20%, occurring when the mean power of noise is as large as the mean power of waveforms (0 dB noise). Flexibility of the proposed model is tested using waveforms simulated under spatially varying EC, and the EC variations along a TDR waveguide can be detected by the proposed model. In summary, the proposed model provides reliable EC estimations, and it can evaluate uniform or varying EC distributions along a TDR waveguide under uniform moisture conditions. This model can be imbedded into the TL-BMO model for integrated water content and EC determination for commonly measured (251-scanning point) TDR waveforms.

Keywords

Electrical conductivity, Inverse modelling, Time domain reflectometry, Waveform interpretation

Disciplines

Agriculture | Earth Sciences | Electrical and Computer Engineering

Comments

This article is published as Wang, Zhuangji, Dennis Timlin, Yuki Kojima, Chenyi Luo, Yan Chen, Sanai Li, David Fleisher, Katherine Tully, Vangimalla R. Reddy, and Robert Horton. "A piecewise analysis model for electrical conductivity calculation from time domain reflectometry waveforms." *Computers and Electronics in Agriculture* 182 (2021): 106012. doi: 10.1016/j.compag.2021.106012.

Authors

Zhuangji Wang, Dennis Timlin, Yuki Kojima, Chenyi Luo, Yan Chen, Sanai Li, David Fleisher, Katherine Tully, Vangimalla R. Reddy, and Robert Horton

Computers and Electronics in Agriculture 182 (2021) 106012

Contents lists available at ScienceDirect

Computers and Electronics in Agriculture

journal homepage: www.elsevier.com/locate/compag

Original papers

A piecewise analysis model for electrical conductivity calculation from time domain reflectometry waveforms

Zhuangji Wang [a,b,*], Dennis Timlin [a], Yuki Kojima [c], Chenyi Luo [d], Yan Chen [e], Sanai Li [a], David Fleisher [a], Katherine Tully [b], Vangimalla R. Reddy [a], Robert Horton [f]

[a] Adaptive Cropping System Laboratory, USDA-ARS, Beltsville, MD 20705, USA
[b] Department of Plant Science and Landscape Architecture, University of Maryland, College Park, MD 20742, USA
[c] Department of Civil Engineering, Gifu University, 1-1 Yanagido, Gifu City, Gifu 501-1193, Japan
[d] School of Life Science, Beijing University of Chinese Medicine, Beijing 102488, China
[e] Department of Soil and Water Science, China Agricultural University, Beijing 100193, China
[f] Department of Agronomy, Iowa State University, IA 50011, USA

ARTICLE INFO

Keywords:
Electrical conductivity
Inverse modelling
Time domain reflectometry
Waveform interpretation

ABSTRACT

Electrical conductivity (EC) represents a material's ability to conduct electric current. Soil EC has been used as a soil quality attribute related to soil pH, nutrient availability, crop suitability and soil microbial activity. Time domain reflectometry (TDR) estimates soil water content and EC based on the propagation/reflection and energy attenuation of voltage signals along a waveguide. To maximize the data use efficiency, waveform interpretations for simultaneous water content and EC determination are needed. A tangent line/bounded mean oscillation (TL-BMO) model is available to estimate soil water content from TDR waveforms, but an associated EC model is not yet available. The objectives of this study are (1) to introduce a piecewise analysis method for TDR waveform interpretation, and (2) to develop a model for EC computation along a TDR waveguide under homogeneous water content. The proposed model sequentially fits a TDR waveform for the coaxial cable, the connection, and the waveguide according to the transmission line equation. A TDR waveguide can be discretized into multiple successive pieces for the determination of EC variations along the waveguide. Simplifications of the fitting procedures via (1) existing models, e.g., TL-BMO and Topp et al. (1988) models, and (2) analysis of waveforms obtained from controlled conditions, e.g., in distilled water under room temperature (~20 °C) and air pressure (~101 kPa), are also applied. Accuracy and stability of the proposed model are tested via observed TDR waveforms obtained under uniform EC conditions but perturbated with a range of noise levels. EC values computed with only one discretized piece (i.e., no discretization along the waveguide) are consistent with the theoretical EC values, and the results are robust for all of the tested noise levels. As the number of discretized pieces and the noise levels increase, numerical oscillations in the results increase. The maximum relative errors are <20%, occurring when the mean power of noise is as large as the mean power of waveforms (0 dB noise). Flexibility of the proposed model is tested using waveforms simulated under spatially varying EC, and the EC variations along a TDR waveguide can be detected by the proposed model. In summary, the proposed model provides reliable EC estimations, and it can evaluate uniform or varying EC distributions along a TDR waveguide under uniform moisture conditions. This model can be imbedded into the TL-BMO model for integrated water content and EC determination for commonly measured (251-scanning point) TDR waveforms.

1. Introduction

Electrical conductivity [EC (abbr. in text, hereinafter), σ (abbr. in equations, hereinafter), mS cm^{-1}] values represent a material's ability to carry electric current. Soil EC varies with respect to water content and soil solution concentration, and it partially reflects the osmotic potential and ionic strength of a soil solution, which relate to soil water and nutrient availability for crop growth (Griffin and Jurinak, 1973; Corwin and Lesch, 2005). For instance, Mirzakhaninafchi et al. (2017) reported the correlations among soil EC, soil water content and soil nitrogen

* Corresponding author at: Adaptive Cropping System Laboratory, USDA-ARS, Beltsville, MD 20705, USA.
E-mail addresses: cauwzj@gmail.com, zhuangji.wang@usda.gov (Z. Wang).

https://doi.org/10.1016/j.compag.2021.106012
Received 11 September 2020; Received in revised form 19 January 2021; Accepted 20 January 2021
Available online 12 February 2021

levels in multiple soil types. Since measuring soil EC is relatively simple and quick, EC becomes a commonly used soil quality indicator, especially for anthropogenic manipulations of soil. For example, Peng et al. (2019) and Coppola et al. (2016) performed crop water demand predictions, irrigation optimizations and soil salinity controls based on soil EC measurements; Sanches et al. (2018) used EC values as a reference to adjust soil pH via lime additions; Yang et al. (2019) and Luo et al. (2020) measured EC variations of highway roadside soil samples following concrete surface grinding to assess the effects of concrete waste on soil chemical properties and plant growth. In addition, continuous EC measurements over time with specific tracers, e.g., KCl or $CaCl_2$, are used to study soil chemical transport properties and provide breakthrough curves for a range of soil types under a variety of managed field conditions, such as compaction or tillage (Gaur et al., 2007; Heitman et al., 2007).

Traditional methods of EC measurements are based on soil liquid extractions. With the development of electromagnetic techniques, sensors are applied for in situ and non-destructive measurements of soil EC and volumetric water content [VWC (abbr. in text, hereinafter), θ_v (abbr. in equations, hereinafter), $cm^3\ cm^{-3}$]. Time domain reflectometry (TDR), frequency domain reflectometry (FDR, or frequency domain analysis of TDR measurements) and ground conductivity meter (GCM) are three commonly used sensors. GCM is a contactless sensor suitable for large area survey, while TDR and FDR are local-scale measurements (Mazurek and Putynkowski, 2016). TDR measurements are based on propagation/reflection of voltage signals along parallel waveguide rods (Noborio, 2001; Robinson et al., 2003; Lu et al., 2017; Tian et al., 2018). Propagation speed and energy attenuation of voltage signals correspond to relative permittivity (ε_r) and EC in material surrounding the TDR waveguide (Schwartz et al., 2013). Compared to FDR, TDR follows a relatively simple physical theory, without the need of convolution and Fourier transforms (Heimovaara, 1994; Minet et al., 2010), and TDR sensor calibrations are easier than those for FDR (Agah et al., 2019).

Given a TDR sensor, the direct output of TDR measurements is the voltage (U) observed at the source point of the coaxial cable, and TDR devices display U as a "reflection coefficients (u)", where $u = U/U_0 - 1$ and U_0 is the input voltage. A TDR waveform is defined as the variation of $u(t)$ with respect to time (t) within a pre-specified time window, from a time point before a voltage signal enters the waveguide to a time point after the reflected voltage leaves the waveguide. Based on the signal rise-time and sampling frequency, to obtain stable measurements, relatively long waveguide rods (~150 mm) are often used in commercial TDR systems. Recent designs of TDR sensors use relatively short waveguide rods for measurements near soil surface (~70 mm, e.g., Peng et al., 2019). In order to perform effective TDR measurements and data analysis with short waveguide rods, a rapid pulse excitation of the voltage signal and a high sampling frequency of U are needed.

Numerical procedures of deriving VWC and EC from TDR waveforms have evolved over time. A recently developed tangent line/second order bounded mean oscillation (TL-BMO) model applied a BMO operator to determine the second order derivative of TDR waveforms, and combined with the tangent line method (Topp et al., 1980) as a prediction-correction model (Wang et al., 2014; Wang et al., 2016). TL-BMO has been used as an accurate and stable model to determine ε_r and VWC (Wang et al., 2017). To maximize the data use efficiency of TDR measurements, simultaneous determination of VWC and EC is important; however, current version of TL-BMO only supports determination of ε_r and VWC. Thus, one goal of this study is to establish a new waveform interpretation model for EC determination.

Numerical models for EC determination from TDR waveforms were initiated in 1970s (Giese and Tiemann, 1975). Dalton et al. (1984) and Topp et al. (1988) computed EC with the input voltage, as well as two voltage values before and after the second reflections in TDR waveforms. Yanuka et al. (1988) refined the calculation by including voltage values from the multiple-reflection sections of TDR waveforms. Alternatively, Nadler et al. (1991) proposed an approach to estimate EC with impedance, cell constant and temperature. One similarity shared among the three models is that the calculation of EC relies on voltage values directly obtained from TDR waveforms. Therefore, they are referred to as direct models. The quality of the direct models varies with TDR sensors, signal generator, computation procedures and EC values to be determined. For example, Munoz-Carpena et al. (2005) reported constant offsets between the theoretical EC values and the TDR EC values calculated via the Topp et al. (1988) or Dalton et al. (1984) models. The Giese and Tienman (1975) method worked well for relatively small EC values, and error compensation was required for relatively large EC values. Recent studies focused on investigating the error sources of the direct models and provided improvements. For example, Lin et al. (2008) identified the influences of cable resistance, errors in signal generators, and scaling of reflection coefficients on the EC computation via direct models. Shuai et al. (2017) improved the derivation of EC using a model of steady state reflection coefficients based on multi-section transmission line theory.

Inverse modelling is an alternative way to interpret TDR waveforms. For inverse modelling, the transmission line equation (also referred to as the "telegraph equation", Ramo et al., 1984) is applied to simulated waveforms ($\widehat{u}$) with TDR electrical parameters, i.e., capacitance (C), inductance (L), resistance along TDR sensors (R), and resistance (of the medium) between parallel waveguide rods (G). The goal of inverse modelling is to achieve a best fit of a simulated waveform to a measured waveform by adaptively choosing C, L, R and G values. The optimal C, L, R and G values obtained from the fitting process can be used to derive EC and VWC. Although both VWC and EC can be solved, the focus of existing inverse models has mainly been placed on the determination of VWC distributions along a TDR waveguide.

During the development of inverse models, several designs based on time-domain integrations have been explored. For example, Yanuka et al. (1988) discretized the TDR waveguide into multiple pieces and simulated stepwise waveforms with electrical parameters estimated within each piece. Timlin and Pachepsky (1996) introduced an inertia factor to count for the rise-time and applied genetic algorithms to optimize the electrical parameters. Todoroff et al. (1998) decomposed the electrical field into forward and backward travelling waves and performed inverse analysis by superpositions of the backward, i.e., reflected, wave components. In addition to the integration models, Oswald et al. (2003) and Greco (2006) directly solved the differential formulation of the telegraph equation to obtain simulated waveforms, and minimized the Euclidean distance ($\mathscr{L}^2$) between measured and simulated waveforms. Compared with the direct models, inverse modelling processes the calculations using the entire waveform, making the waveform interpretation relatively robust. Inverse modelling converts the TDR waveform fitting to an optimization (minimization) problem, where existing algorithms and regulation techniques can be directly applied. Moreover, inverse modelling is compatible with varying VWC or EC along a TDR waveguide, while direct models usually provide one intermediate value of VWC and EC along a TDR waveguide (Ochiai et al., 2010).

Inverse modelling, however, does have drawbacks. One difficulty is that TDR waveforms only present "single-side" voltage results. Although voltage varies with respect to time and spatial location along the TDR waveguide, as voltage propagates within a given TDR sensor, only voltage values at the source point are recorded, rather than spatial voltage distributions. However, for optimal fitting, C, L, R and G are allowed to vary along the TDR waveguide. Thus, the degrees of freedom included in inverse modelling can potentially exceed the constraints provided by the number of voltage (or reflection coefficients) data from TDR waveforms. To mitigate such an under-determined problem, regulations are applied. For example, Oswald et al. (2003) added a penalty term, $\int_t \left[a\left\|\frac{d}{dt}\widehat{u}\right\|^2 + b\left\|\frac{d^2}{dt^2}\widehat{u}\right\|^2 \right] dt$, to the $\mathscr{L}^2$-distance between measured and simulated waveforms to enhance the numerical stability of the

minimization procedures. Greco (2006) parameterized the spatial distributions of VWC along a TDR waveguide using a sigmoid function, which significantly reduced the number of parameters to be fitted; however, the flexibility and generalizability of that inverse model were limited. Therefore, Greco (2006) mainly used the model to describe wetting and drying fronts during soil water infiltration and evaporation.

Except for special cases (Rashidinia et al., 2014; Raftari and Yildirim, 2010; Adewumi et al., 2017), genetic algorithms have been used in the numerical implementations for inverse modeling to address problems with relatively large degrees of freedom and non-uniqueness of optimal solutions. Hence, the computational load for inverse models can be relatively heavy. Although some modifications with gradient descents have been proposed, such as Requena-Pérez et al. (2006), genetic algorithms are still the dominant process, while gradient descents are applied to refine the results from genetic algorithms. Thus, based on the shortcomings of the existing algorithms, there is a need to improve TDR inverse modelling.

Following the ideas of TDR inverse models, the objectives of this study are (1) to introduce a piecewise analysis method for TDR waveform interpretation; and (2) to develop a model for EC computation. Some pre-treatments for the proposed model are also included to facilitate fast computation. A computer program based on MATLAB (MathWorks, Inc.) is used for model implementation. The proposed model can be combined with the TL-BMO model to provide an integrated waveform interpretation. The composition of this paper is as follows: in Section 2, TDR theory and model establishment are provided; in Section 3, the proposed model is tested with observed waveforms and numerical examples; Section 4 provides a general summary with some potential applications and future research topics of the piecewise analysis model.

2. Model development

We first provide a general introduction to a TDR measurement system (Section 2.1), followed by the concept of TDR piecewise analysis (Section 2.2). In the newly proposed model, the intensive computational loads that occur in existing inverse models are circumvented by using (1) direct model results and (2) calibration measurements, e.g., TDR waveforms measured in distilled water (EC ≈ 0 mS cm^{-1}). Those two approaches are used as pretreatments for the proposed piecewise model. The numerical implementation of the proposed model is explained with examples (Sections 2.3 and 2.4), and a simple computer program based on MATLAB is developed to perform the piecewise analysis. Because this model can be designed as a subroutine of TL-BMO, soil VWC is assumed to be uniform; however, the EC value is assumed to be either uniform or have spatial variations along a TDR waveguide.

2.1. Governing equations of voltage signals in TDR

A typical TDR system includes a signal generator, which generates a voltage signal and records the reflected voltage, and one or more TDR sensors, where each sensor has a waveguide that usually contains two parallel rods of length ℓ_p. A TDR sensor uses coaxial cable to connect the signal generator to the waveguide, and the waveguide rods are the portions of the TDR sensors buried to have direct contact with soil or other medium to be measured. A diagram of a TDR system is shown in Fig. 1.

Suppose the x-axis is set along the TDR sensor (Fig. 2). The "source point" ($x = 0$) indicates the connection between the signal generator and the coaxial cable; the "loading point" ($x = X$) indicates the far-right endpoint of the waveguide. We also refer to the "source point of waveguide" as the junction between the connection and the waveguide ($x = x_{m2}$).

In Fig. 1-a, each small element of the TDR sensor (Δx) can be considered as the electrical circuit shown in Fig. 1-b. Based on the Kirchhoff Circuit Law, the governing equation of voltage signal travelling along a TDR sensor is described by the telegraph equation (Ramo et al., 1984).

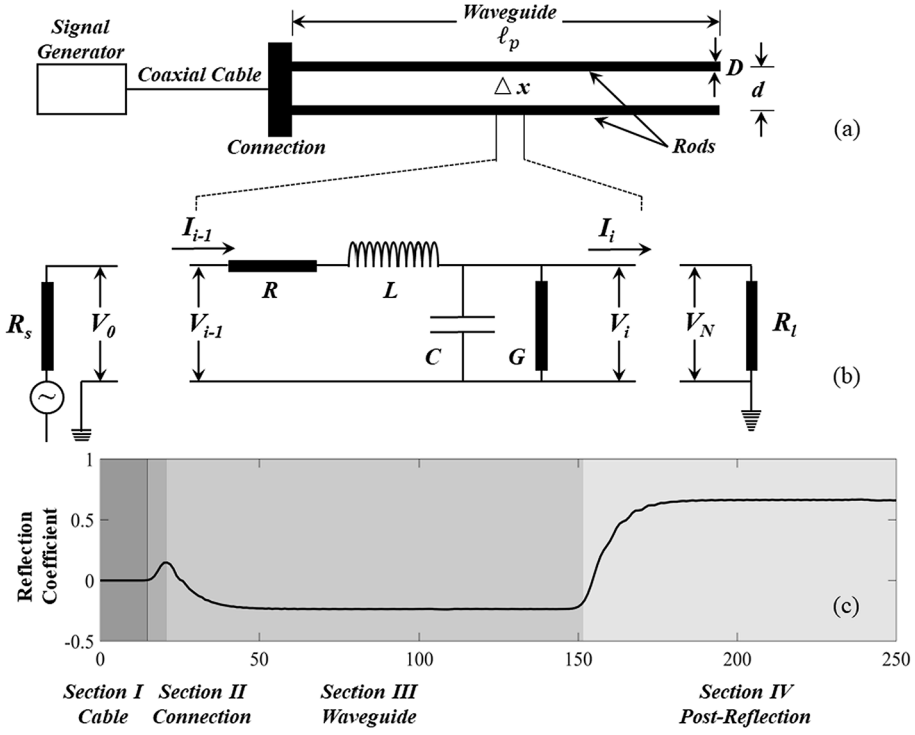

Fig. 1. A diagram of a TDR system (a) with an electrical circuit model of voltage propagation along a TDR sensor (b) and a simulated TDR waveform in distilled water (c, $\varepsilon_r = 80.5$, $EC \approx 0$ mS cm^{-1}).

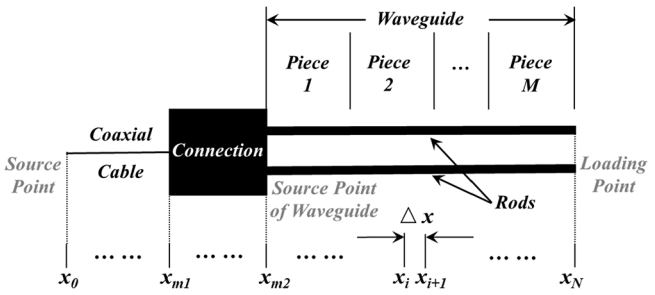

Fig. 2. A piecewise discretization of a TDR sensor is shown with the coordinates for coaxial cable, connection and waveguide (with two parallel rods) marked. In a heterogeneous medium, the waveguide can also be divided into M pieces, and EC values can be computed for each piece sequentially. The locations of "source point", "loading point" and "source point of waveguide" are also presented in this figure.

$$\begin{cases} \dfrac{\partial U}{\partial x} = -\left[R(x) + L(x)\dfrac{\partial}{\partial t}\right] I \\ \dfrac{\partial I}{\partial x} = -\left[G(x) + C(x)\dfrac{\partial}{\partial t}\right] U \end{cases} \tag{1}$$

where $U = U(x,t)$ and $I = I(x,t)$ are voltage and current functions for both spatial coordinates (x) and time (t). The four electrical parameters are also presented as functions of space (x), i.e., $L(x)$, $R(x)$, $C(x)$ and $G(x)$. Within the coaxial cable, L, R, C and G can be assumed as constants, provided by the manufacturer via characteristic impendence and velocity of propagation. For the TDR waveguide, based on a two-wire transmission line model (Ramo et al., 1984), $L(x)$, $R(x)$, $C(x)$ and $G(x)$ are functions of the materials and the geometrical configurations of waveguide rods. In addition, $C(x)$ and $G(x)$ are related to EC and dielectric permittivity values of the medium surrounding the TDR waveguide.

$$\begin{cases} R(x) = \dfrac{2R_{skin}}{\pi D} \times \dfrac{d/D}{\sqrt{(d/D)^2 - 1}} \\ L(x) = \dfrac{\mu}{\pi}\cosh^{-1}\left(\dfrac{d}{D}\right) \\ G(x) = \left(\dfrac{\pi\sigma(x)}{\cosh^{-1}(d/D)}\right) + \left(\dfrac{\pi\omega\varepsilon''(x)}{\cosh^{-1}(d/D)}\right) \\ C(x) = \left(\dfrac{\pi\varepsilon(x)}{\cosh^{-1}(d/D)}\right) \end{cases} \tag{2}$$

In Eq. (2), D represents the diameter of one waveguide rod, while d is the distance between the two parallel rods (Fig. 1-b); R_{skin}, the skin resistance, appears for high frequency signals; μ is the magnetic permeability; ω represents signal frequency; ε and ε'' are real and imaginary parts of the dielectric permittivity. Except for measurements in clayey soil, we can assume $\varepsilon'' \approx 0$ and $\varepsilon = \varepsilon_r\varepsilon_0$, i.e., the product of relative permittivity and the permittivity in a vacuum (Oswald et al., 2003). EC appears in the resistance G. Hence, the evaluation of G in a TDR waveguide is the focal point for EC computation.

The pulse excitation of the voltage signal (U_s) from the signal generator is written into the boundary condition at the source point (Oswald et al., 2003); and U_s is assumed to follow an exponential relation with respect to time (Greco, 2006), i.e., $U_s = \widetilde{U}[1 - \exp(-bt)]$. $\widetilde{U}$ is the target voltage and b is a parameter related to the rise-time. For the boundary condition at the loading point, the only input is the voltage injected into the waveguide. Both boundary conditions are summarized using Ohm's Law, and shown in Eq. (3).

$$\begin{cases} Source\ \ Point: I(x=0,t) = \dfrac{U_s - U(x=0,t)}{R_s} \\ Loading\ \ Point: I(x=X,t) = \dfrac{U(x=X,t)}{R_l} \end{cases} \tag{3}$$

In Eq. (3), R_s and R_l are the source resistance (internal resistance of the signal generator) and loading resistance, respectively. Based on Ohm's Law at the source point, the input voltage to the TDR sensor U_0 is not equal to U_s. Instead, U_0 is a fraction of U_s, depending on the source resistance and the impedance of the coaxial cable Z_c, i.e., $U_0 = \frac{Z_c}{Z_c+R_s}U_s$.

The telegraph equation (Eq. (1)), together with the boundary conditions (Eq. (3)), can be numerically solved with finite difference schemes. TDR waveforms are obtained by recording the voltage values at the source point of the TDR sensor. A simulated waveform in distilled water is shown in Fig. 1-c.

In general, a TDR waveform can be divided into four sections (Fig. 1-c). Section I presents reflection coefficients when voltage travels along the coaxial cable, i.e., from 0 to x_{m1} in Fig. 2. Section II presents the reflection coefficients when voltage signal is within the connection between the coaxial cable and the waveguide, i.e., from x_{m1} to x_{m2}. The coaxial cable and the waveguide rods are soldered together within the connection, where measurable changes in the electrical properties occur. A portion of the voltage signal is reflected due to the discontinuity of electrical properties, leading to a steep increase in reflection coefficients, i.e., the first reflection position of the TDR waveform (t_1). Section III presents the reflection coefficients when voltage propagates along the waveguide, between x_{m2} to X, where C and G are directly related to the soil VWC and EC. In a homogeneous medium, such as distilled water shown in Fig. 1-c, constant C and G values can be assumed; while in a heterogeneous medium, the propagation speed or energy attenuation of the voltage signal may vary along the waveguide, leading to pattern changes within Section III. When voltage reaches the loading point of the TDR sensor, it reflects and propagates back to the source point, resulting in an increasing trend of reflection coefficients at the end of Section III, i.e., the second reflection position of the TDR waveforms (t_2). The variations of the reflection coefficients within Section IV is subjected to multi-reflections.

2.2. The concept of TDR piecewise analysis

In existing inverse models, four electrical parameters, L, R, C and G are estimated simultaneously along a TDR waveguide, which results in a high dimensional minimization problem. Moreover, model flexibility is emphasized by performing the inverse fitting only based on measured waveforms, without any a priori knowledge. That can limit the computing performance of an inverse model. Thus, the proposed piecewise model attempts to optimally leverage model flexibility and efficiency.

The idea of TDR piecewise analysis is to approximate the voltage propagation along three segments, i.e., coaxial cable, connection and waveguide (Fig. 2), and sequentially determine the electrical parameters of each segment. Voltages travelling within the segments correspond to the waveforms in Section I, II and III, respectively (Fig. 1). Since TDR is a causal system, changing the electrical parameters in later segments will not alter the waveform in former sections. Analogous to the piecewise analysis idea, a TDR waveguide can also be discretized into multiple pieces (Fig. 2), and the electrical parameters, especially G in this study, can be determined by successively fitting piece-by-piece from the source point of waveguide to the loading point.

Based on Eq. (2), some of the electrical parameters, such as L and R, are specific for each TDR sensor, and they can be characterized from independent measurements. Because calibrating the waveguide length in distilled water is commonly performed before measurements, such calibration waveforms can be used as an independent dataset to evaluate L and R. Then, the L and R values can be parameterized for piecewise

analysis and EC computation for waveforms obtained later with the same TDR sensor.

In addition, applications of direct models for individual waveforms can also provide a priori knowledge for piecewise analysis. For example, the TL-BMO model combines the tangent line method with a BMO gradient operator (Wang et al., 2014; Chen et al., 2013) to calculate soil VWC; while the Topp et al. (1988) equation provides estimations of EC values from TDR waveforms with (constant) system errors. Under the assumption that VWC is uniform along a TDR waveguide, VWC estimated by TL-BMO can be used to provide a first approximation of C; and EC calculated with the Topp et al. (1988) equation can demarcate a searching interval for G.

Effective error control is necessary for the piecewise analysis because numerical errors may accumulate or even enlarge during the sequential fitting. We propose the following cost function to measure the differences between simulated waveforms ($\hat{u}$) and measured waveforms (u).

$$\begin{aligned} &\min L(\hat{u},u) = \mathscr{L}^2(\hat{u},u) + \alpha\mathscr{L}^2\left(\frac{d\hat{u}}{dt},\frac{du}{dt}\right) \\ &\text{s.t.}: Corr(\hat{u},u) > \beta \end{aligned} \tag{4}$$

$\mathscr{L}^2(\cdot,\cdot)$ indicates the Euclidean distance between measured and simulated waveforms or between their derivatives. $Corr(\hat{u},u)$ represents the correlation coefficient between $\hat{u}$ and u, which regulates the shape of $\hat{u}$. The usage of $Corr(\hat{u},u)$ as a shape factor, instead of directly comparing the second order derivatives of $\hat{u}$ and u, is done because $Corr(\hat{u},u)$ is relatively robust against random noise. Similarly, $\frac{du}{dt}$ is not directly computed from measured waveforms but is calculated with a polynomial smoothing process (i.e., Savitzky-Golay filter). Numerical methods in solving Eq. (4) depend on the sources of the TDR waveforms (i.e., from calibration measurements or EC measurements), and the solving procedures are provided in Sections 2.3 and 2.4 with examples.

2.3. Initial estimations of electrical parameters with calibration (distilled water) waveforms

Fitting the calibration waveforms measured in distilled water (EC ≈ 0 mS cm^{-1}) not only provides an initial estimation of the electrical parameters, but also provides some information for the geometrical configurations of TDR sensors, e.g., the length of coaxial cables included in observed waveforms and the length of waveguide rods.

Fitting procedures of TDR piecewise analysis are shown in Fig. 3. A measured TDR waveform is presented as a thick gray curve. Three fitting steps, corresponding to Sections I, II and III of the given waveform, are used to determine the electrical parameters for the coaxial cable, connection and waveguide.

Because the length of the coaxial cable for an individual TDR sensor can be arbitrary and the window length for presenting TDR waveforms is usually based on the span of Section III, the reflection coefficients presented in Section I only associate with a portion of the coaxial cable near the waveguide rods. Thus, the goal for fitting Section I is to determine an apparent length of the coaxial cable (a pseudo coaxial cable length) used in the piecewise analysis model, such that the voltage signal can be fully established within the cable. The apparent length should be large enough to cover the time period for the excitation of the voltage signal (rise-time), and it should be smaller than the actual coaxial cable length. Because after the rise-time, the voltage signal will travel stably within the coaxial cable until reach the connection, which is not important in waveform fitting. Choosing a short apparent length can avoid solving the telegraph equation during that stable traveling time period, hence reduce the computing load. Based on the characteristic impedance and the velocity of propagation of the coaxial cable, the reflection coefficients when voltage propagate along the coaxial cable can be simulated based on Eq. (1). When the input voltage is fully established and a constant reflection coefficient is reached, the corresponding time period is the rise-time. The sum of rise-time and the time period associated with

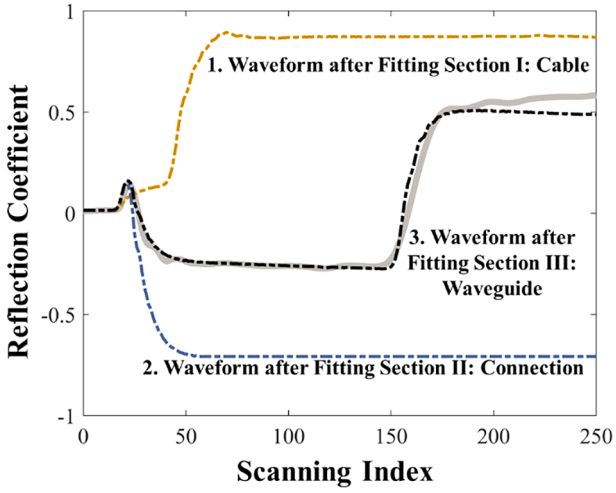

Fig. 3. Fitting for a calibration waveform using TDR piecewise analysis. The waveform was obtained within distilled water (EC ≈ 0 mS cm^{-1}), room temperature (~20 °C) and room air pressure (~101 kPa). The thick gray curve represents the measured waveform; while the three dashed curves are three intermediate steps during the piecewise analysis, representing the simulated waveform after fitting the coaxial cable segment, connection segment, and waveguide segment.

Section I can be converted to the apparent cable length using the velocity of propagation. For Section II, the impedance of the connection can be determined based on the local maximum of the reflection coefficient and the impedance of the coaxial cable. Then, the waveform within Section II can be reconstructed based on the impedance value of the connection. The electrical parameters of the coaxial cable and the connection obtained via waveform fitting in Section I and II can be used in other waveforms measured with the same sensor and signal generator.

Waveform fitting for Section III is performed using a gradient descent procedure derivate based on $L(\hat{u},u)$ in Eq. (4). An appropriate initialization of the electrical parameters has effects on the performance of waveform fitting and parameter optimization. The initial values of L and R can be calculated based on the material and the geometrical configurations of waveguide rods, shown in Eq. (2). VWC determined by the TL-BMO model, and the EC value determined from the Topp et al. (1988) equation can be used to initialize C and G. The evolution of electrical parameters follows:

$$X_{n+1} := X_n - \lambda\partial_X L(\hat{u},u) \approx X_n - \lambda\frac{[L(X_n+\delta X) - L(X_n)]}{\delta X} \tag{5}$$

In Eq. (5), $X = L,R,C,G$ and δX is a small perturbation of the electrical parameters; λ represents the learning speed; n is the iteration step. We implicitly use the fact that although $L(\hat{u},u)$ in Eq. (4) is defined based on $\hat{u}$ and u, it is a function of L, R,C and G based on Eqs. (1) and (3). Taking derivatives directly is impossible because $\hat{u}$ is simulated with Eqs. (1) and (3). Therefore, an approximation based on a finite difference scheme should be used.

After waveform fitting with the gradient descent procedures, the optimal electrical parameters are artificially perturbated by ±10%, and the simulated waveform that maximizes $Corr(\hat{u},u)$ in Eq. (4) is adopted as the final result. Such a refinement based on $Corr(\hat{u},u)$ can enhance the numerical stability of the computation. The optimal L and R of the waveguide rods following the inverse fitting can be considered as constants for the specific TDR sensor, and used for other waveforms measured with the same TDR sensor.

Nearly all the electrical parameters are obtained through the waveform fitting from Section I to III. That will also provide the positions of t_2 in simulated waveforms, but the increasing trend of reflection coefficients in simulated waveforms after t_2 (in Section IV) may not be the same as in the measured waveforms. In order to correct that, Section IV

has to be fitted and R_l in Eq. (3) should be optimized. However, optimizing R_l is not related to the estimation of EC along the waveguide. Therefore, we omit that optimization and accept the differences between the simulated and measured waveforms in Section IV.

2.4. Implementation of TDR piecewise analysis for EC computation

The procedures for the EC computation are shown in Fig. 4. Since the electrical parameters of the coaxial cable and the connection are predetermined using the calibration dataset in Section 2.3, fitting for Sections I and II of the waveforms are omitted. For demonstration purposes, the waveguide is assumed to be divided into two pieces, based on the scheme shown in Fig. 2.

Since L and R of the waveguide rods are provided in Section 3.2, and VWC is uniform along the waveguide, a simple bisection method can be applied to minimize the cost function $L(\hat{u},u)$ in Eq. (4), and determine the corresponding values of G, hence EC. For the bisection method, when the optimal solution is within a given interval, the interval can be subdivided into two sub-intervals, and the optimal solution has to be within one of the two sub-intervals, which can be subdivided in the next steps. Iteratively, the length of the sub-interval will decrease geometrically, and boundary points of the sub-interval will approach to the optimal solution. Thus, the average of the boundary points will be reported as an approximation to the optimal solution. The convergence of the bisection method is based on the nested-interval theorem.

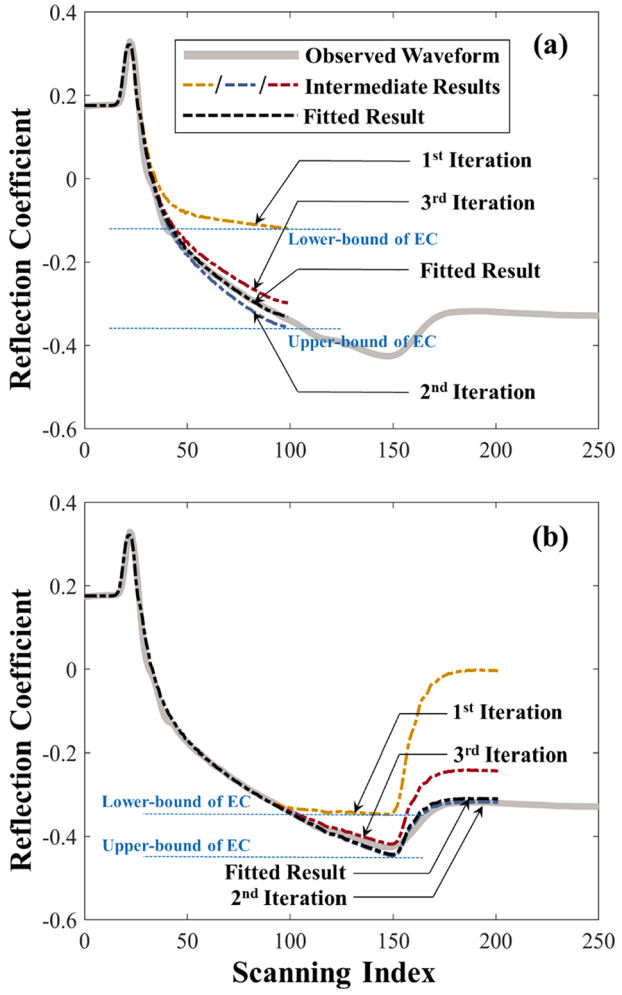

Fig. 4. Waveform fitting for EC = 3.0 mS cm^{-1} via TDR piecewise analysis. The thick gray curve represents the measured waveform. The waveguide is divided into two pieces, and the calculation of EC values for the Piece 1 (a) and Piece 2 (b) are performed successively.

For example, in Fig. 4-a, the initial EC value of Piece 1, obtained from direct method for the whole waveform, is smaller than the true value, such that the simulated waveform appears to be above the measured waveform for the first iteration. After the EC value is increased, the simulated reflection coefficients decrease, and the simulated waveform appears to be below the measured waveform, shown as the second iteration. Those two EC values demarcate the upper and lower bounds for the true EC within Piece 1. For the following iterations, the averaged EC value of the two previous EC bounds is adopted as a new approximation. If the simulated waveform is above the measured waveform, then the EC value used in the current iteration step becomes a new lower EC bound; if the simulated waveform is below the measured waveform, then the previous upper EC bound is substituted by the averaged EC value. After the optimal parameters are selected, an artificial perturbation similar to the one mentioned in Section 2.3 is performed to select the final result which maximizes $Corr(\hat{u},u)$.

Similar fitting procedures are performed for Piece 2. In Fig. 4-b, the simulated waveforms for the three iterations and the upper and lower bounds of EC are indicated. In the refinement process, if the difference between the EC value selected based on the $L(\hat{u},u)$ and the EC value that maximizes $Corr(\hat{u},u)$ becomes relatively large (~10%), a weighted average of EC values selected before and after refinement is used. The target of using a weighted average is to control error propagations and improve numerical stability, which usually occurs when EC is heterogeneous within a single piece. For the piece next to the source point of waveguide, e.g., Piece 1 in Fig. 4, relatively small EC values receive relatively large weights. For the following pieces, relatively large weights are assigned to the EC values similar to the computed EC values in the upstream pieces. That "up-wind" manipulation, i.e., data from upstream directions receives larger weights, controls the error propagation by reducing the total variation of the EC along the waveguide, which can be analogized to the "up-wind" scheme in wave equations.

A MATLAB-based (MathWorks, Inc.) computer program was developed to implement the proposed piecewise analysis model. The direct models, such as the TL-BMO and the Topp et al. (1988) model, are also included to provide a priori information for EC evaluation. The statistical/machine learning toolbox and the parallel computing toolbox embedded in MATLAB are applied to enhance the performance of the computer program.

3. Illustrative examples

The piecewise analysis model was first tested with waveforms measured under pre-specified, uniform EC conditions (Section 3.1). The benefit was the pre-specified EC values ("true EC values") were known before TDR measurements, such that the accuracy of the piecewise analysis model could be directly evaluated. EC values determined by the piecewise analysis model should be similar to the true EC values, independent of the number of pieces selected along the waveguide. Noise was added to the observed waveforms to illustrate the numerical stability of the piecewise analysis model. Because the EC values for each piece were estimated sequentially, the piecewise analysis model could be flexible to fit some EC variations along the waveguide. That flexibility was tested in the second example (Section 3.2), where simulated waveforms under varying EC conditions were used, and some noise was added to downgrade the quality of the simulated waveforms. For demonstration of model performance, all the illustrative examples were run on a laptop with an Intel(R) Core (TM) i7-8665U CPU, with Turbo Boost turned off.

3.1. Evaluation of model consistency and stability

TDR waveforms were obtained from a laboratory measurement in $CaCl_2$ solutions. Measurements were performed at room temperature

(~20 °C) and air pressure (~101 kPa). The concentrations of $CaCl_2$ solutions were calculated based on pre-specified EC values (1 and 3 mS cm^{-1}). Then, the EC values were validated with a Hanna HI-4522 EC meter (Hanna Instruments). The TDR sensor had a 150-mm long and 3-mm diameter 2-rod waveguide, and the distance between the parallel rods was 30 mm. The waveguide was connected to a Tektronix 1502B cable tester (signal generator) via 75 Ω coaxial cables (RG-187A/U). For each $CaCl_2$ solution, 20 waveforms were collected. Twenty calibration waveforms in distilled water (EC ≈ 0 mS cm^{-1}) were also obtained. Example waveforms from the measurements are shown in Fig. 5.

Fig. 6 presents the EC values determined by the piecewise analysis model when EC = 1 and 3 mS cm^{-1}. The horizontal axis indicates that the waveguide was discretized into 1–4 pieces, based on the scheme shown in Fig. 2. For each type of discretization, the piecewise EC values are presented successively from the source point of waveguide to the loading point, i.e., from the 1st piece to the M^{th} piece shown in Fig. 2, $M = 1, 2, 3, 4$. The error-bars indicate one standard deviation of the computed results. The computing time for inverse fitting is roughly 4–5 s per piece.

In general, the EC values estimated from the waveforms matched the true EC values, with the errors (the relative difference between the mean of TDR estimated values and the true value) < 10% and the coefficients of variation (the ratio of standard deviation to the mean of TDR estimated values) < 5%. If the waveguide was not discretized, i.e., the piece number was 1, and the EC results were similar to the true values, with the smallest standard deviations. The reason is that the whole waveforms within Section III were included for EC evaluation, such that the numerical fluctuation of EC results was minimized. Therefore, compared to the direct models, the advantage of using fitting procedures is shown. As the number of discretized pieces increased, the number of reflection coefficients shared by each piece decreased, such that the effects of noise within the measured waveforms were relatively enlarged. Therefore, the standard deviations increased with respect to the number of discretized pieces.

In order to evaluate the robustness of the proposed model, artificial noise is added to the waveforms at six levels. The magnitudes of the noise are −20, −13, −10, −6, −3 and 0 dB, corresponding to 1%, 5%, 10%, 25%, 50% and 100% of the waveform mean power. 0 dB noise is selected as the maximal level, because noise greater than 0 dB implies the TDR system produced more noise than signal. For actual measured TDR waveforms, noise levels greater than −10 dB are rare.

Fig. 7 presents the EC values calculated with the proposed model. Similar to Fig. 6, the waveguide is discretized into 1–4 pieces. For both EC values, the patterns of the EC results are consistent. If the waveguide

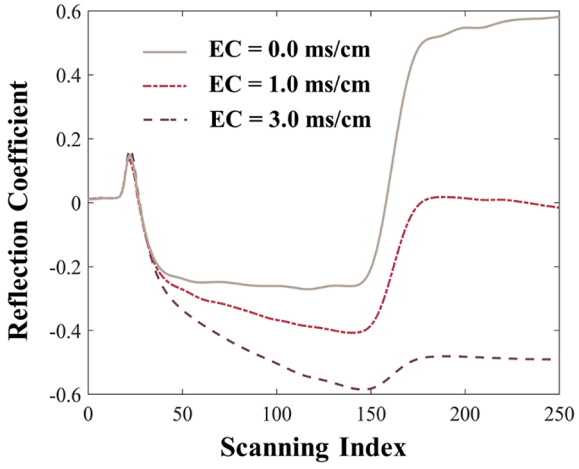

Fig. 5. Sample waveforms measured in $CaCl_2$ solutions with EC = 1 or 3 mS cm^{-1}. The waveform for distilled water with EC≈0 mS cm^{-1} is also shown as a reference.

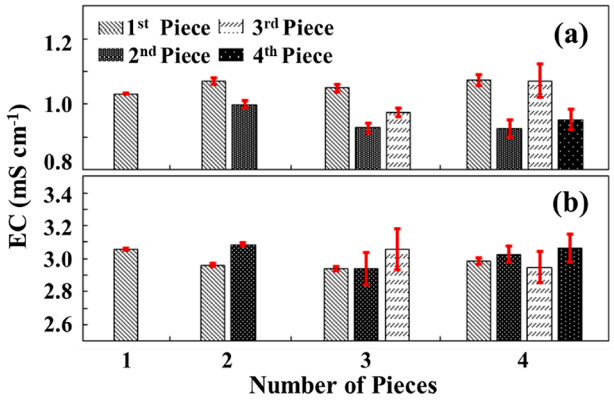

Fig. 6. The EC values derived from measured TDR waveforms when (a) EC = 1 mS cm^{-1} and (b) EC = 3 mS cm^{-1}. The waveguide was discretized into 1, 2, 3 or 4 pieces shown in the horizontal axis. The red error-bars indicate one standard deviation of the computed EC values. (For interpretation of the references to colour in this figure legend, the reader is referred to the web version of this article.)

was not discretized (Fig. 7-a and e), the variations of computed EC, presented by the one standard deviation error-bars, were small even under the largest noise level. That indicates the noise applied to the waveform was smoothed by the fitting processes in the piecewise analysis model. For the results with more than one discretized piece, as the number of pieces increased or the noise level increased, the variations of computed EC for each piece increased. The largest variation (~20% relative error for 0 dB noise) usually occurred at the piece next to the loading point, because the artificial noise not only degraded Section III of the waveforms, but also perturbated the second reflection position (t_2). Both present challenges to the piecewise analysis. However, that situation mainly occurred for noise levels of −6, −3 and 0 dB, which rarely occurred for actual measurements.

3.2. Evaluation of model flexibility

TDR waveforms were simulated with pre-specified EC distributions along the waveguide. An independent model was used to generate the simulated waveforms, and the waveforms were then blurred artificially by including −13 dB noise to degrade the waveform quality, especially at the position where EC values changed. In Fig. 8, two series of EC distributions are shown. Following the labels of the waveforms from to ⑨, Fig. 8-a can be considered as snapshots of EC distributions during an invasion of a high concentration solution from the source point of waveguide; Fig. 8-b shows snapshots during an invasion of a high concentration solution from the loading point. The theoretical EC ("true EC" in Fig. 8) values are shown as black bars in the small diagrams next to the waveform plots, the EC values computed from the TDR waveforms ("TDR EC" in Fig. 8) are presented with red lines.

The changes in EC can occur at arbitrary locations along the waveguide. However, in the piecewise analysis, the discretization is predefined. Thus, the location of EC changes can be either within a piece or at the boundary of two adjoined pieces. In this example, in order to present both cases, the EC changes were located at 1/8, 2/8, … 6/8 and 7/8 of the waveguide, and the waveguide was only discretized into 4 pieces. Thus, in Fig. 8, each segment of red lines (based on the waveguide discretization) corresponds to two black bars (based on EC changing locations).

The TDR EC distributions are shown in Fig. 8. Based on the given discretization of the waveguide, when EC changes occur within a single piece, the piecewise model provides intermediate values based on the true EC values within that piece, such as ③, ⑤ and ⑦; however, the intermediate values are not necessarily equal to the means of the true EC (Ochiai et al., 2010). When EC changes occur at the boundary of two

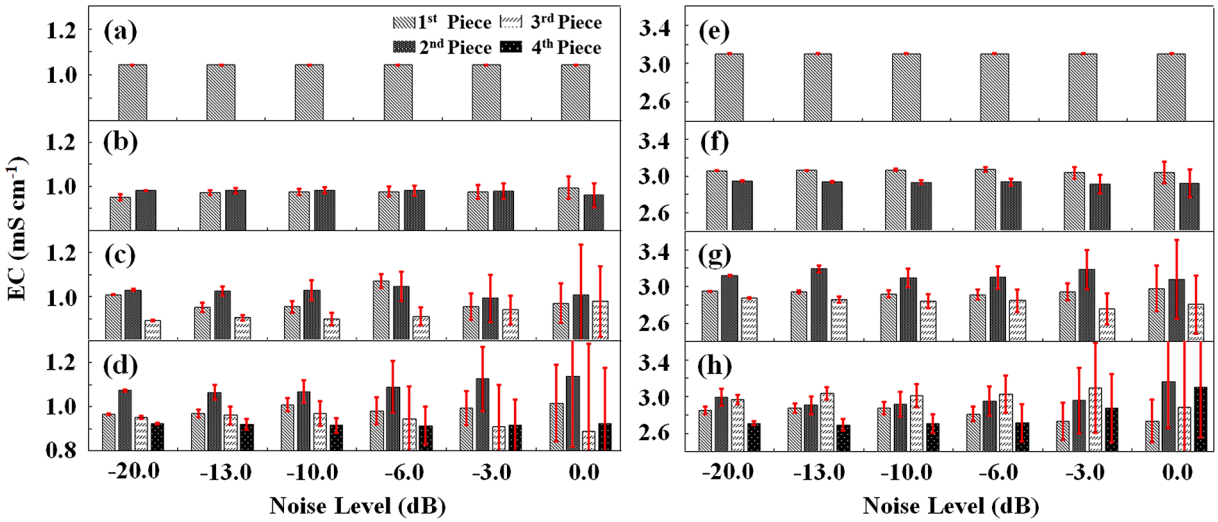

Fig. 7. EC values estimated from TDR waveforms obtained in $CaCl_2$ solutions with EC = 1 mS cm^{-1} (a) to (d) and EC = 3 mS cm^{-1} (e) to (h). The waveguide is divided into 1, 2, 3 or 4 pieces, and the EC values determined for individual pieces are presented in the order from the source point of waveguide to the loading point, i.e., from the 1st piece to the 4th piece. The red error-bars indicate one standard deviation of the EC values, which represent the variations of the computed EC results. (For interpretation of the references to colour in this figure legend, the reader is referred to the web version of this article.)

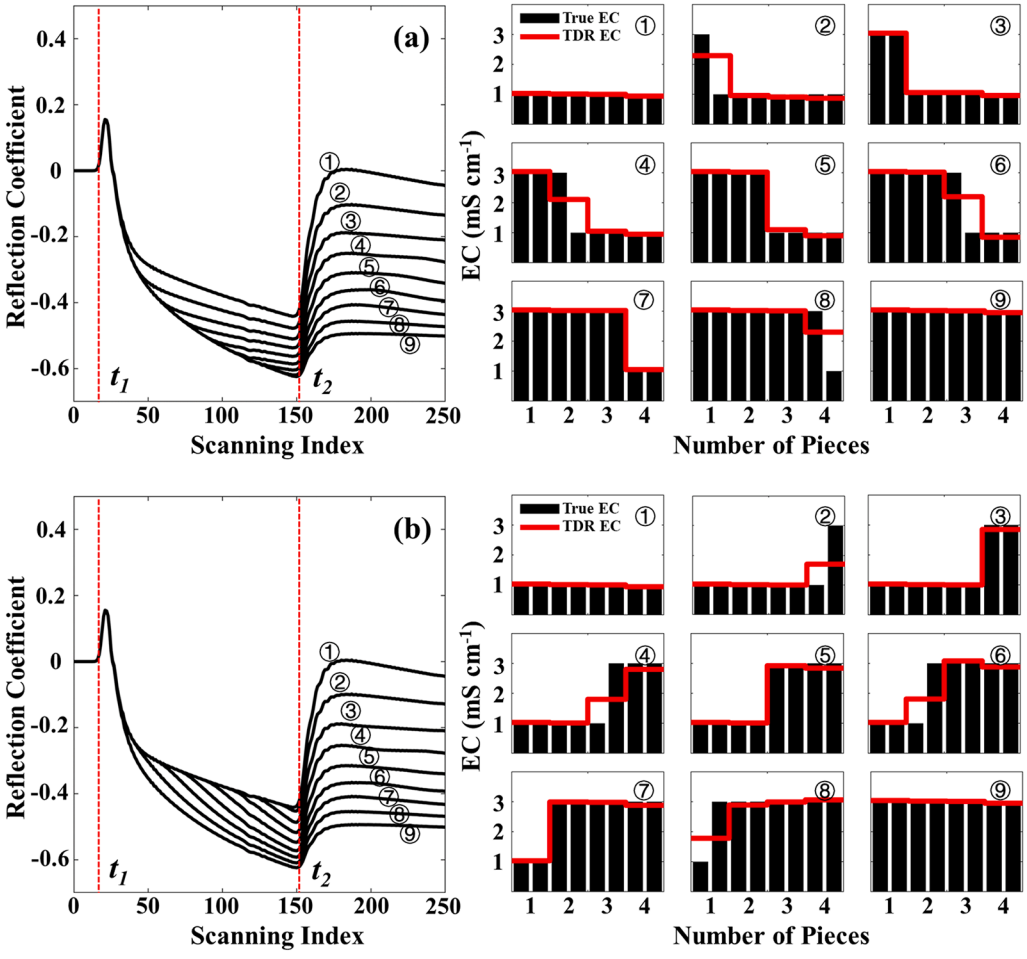

Fig. 8. Two series of simulated waveforms under varying EC conditions are shown in (a) and (b), with the black bars and solid red lines indicating the theoretical EC (true EC) and measured EC (TDR EC) distributions along the waveguide. The true EC changes occurred at 1/8, 2/8, …, 6/8 and 7/8 of the waveguide (8 black bars for each waveform are shown), while the number of pieces indicates that the waveguide is discretized into 4 pieces. The first and second reflection positions (t_1 and t_2) of the waveforms are also marked with red dashed lines. (For interpretation of the references to colour in this figure legend, the reader is referred to the web version of this article.)

pieces, the piecewise analysis results show those changes directly, such as ②, ④, ⑥ and ⑧. Comparing the piecewise EC analysis with the TDR inverse analysis for VWC variations, the location of VWC changes can usually be directly traced, especially using the integration-based methods, such as Timlin and Pachepsky (2002). That is because the VWC changes induce interior reflections within Section III of the waveform, and usually lead to relatively sharp pattern changes of the reflection coefficients, similar to the first or second reflection positions

(t_1 or t_2 in Fig. 8). However, the EC changes do not lead to reflection-type changes, but they slightly alter the slopes of waveforms (refer to TDR waveforms in Fig. 8). Hence, directly tracing the EC changes is difficult. Therefore, the strategy of piecewise analysis in presenting EC variations along the waveguide is to pre-define a spatial frame, i.e., the pieces in Fig. 2, and wait for the EC changes to fall into the spatial frame. The resolution for EC variation is directly related to the number of pieces. For numerical stability, only 4 pieces are used in this example. If the number of voltage (or reflection coefficient) data within Section III can be increased, e.g., by either using longer TDR waveguide rods or increasing the voltage sample frequency, additional pieces can be included in the discretization of waveguide.

4. Summary and conclusion

Time domain reflectometry (TDR) is a widely used technique to determine soil volumetric water content (VWC) and bulk soil electrical conductivity (EC), and the simultaneous determination of VWC and EC from TDR waveforms can maximize data use efficiency. Although the tangent line/second order bounded mean oscillation (TL-BMO) model provides a stable analysis of VWC, its extension for EC computation has not yet been studied. In this study, we introduced a concept of piecewise analysis and developed a model for EC estimation. The model performs sequential fitting procedures, and adopts a priori knowledge from direct models and calibration waveforms to reduce the computational load. A simple MATLAB-based program is developed to perform the piecewise analysis in this study. Accuracy and stability (robustness against noise) of the piecewise model are validated with observed waveforms and waveforms that include a range of artificial noise levels. Relative errors increase as the number of pieces increases (i.e., the number of data points for each piece decreases) or as the noise level increases. However, relative errors are $<20\%$, even for the largest noise level. Flexibility of the piecewise model for spatially varying EC is evaluated with simulated waveforms. Based on the evaluations, the piecewise model can provide reliable EC estimations from TDR waveforms, for both uniform EC conditions and when EC varies along the waveguide. The piecewise model can be implemented within TL-BMO model to provide an integrated soil VWC and EC analysis for commonly measured (251-scanning point) TDR waveforms.

Potential applications of the piecewise model include (1) continuous EC measurements within a uniform medium, e.g., monitoring the EC variations with respect to time in hydroponics (analogy to Section 3.1); and (2) transient EC distribution estimations during laboratory and field solute breakthrough curve measurements made under steady infiltration flux conditions (analogy to Section 3.2). The steady infiltration flux can be achieved via a constant head Mariotte bottle in the laboratory, or by a ponded or tension infiltrometer in the field (Ankeny et al., 1988). Compared to a current multi-depth TDR placement, such as Sheng et al. (2017), or to multi-depth sensors, such as SoilVUE10 (Campbell Scientific, Inc.), the use of a single long TDR sensor with the proposed piecewise model may reduce the disruption of soil profiles during measurements.

The assumption of uniform VWC can be a limitation for general applications of the proposed model. However, addressing EC and VWC variations simultaneously may cause Eq. (4) to be highly non-linear, which increases the complexity in the optimization processes. Learning-based signal or image processing models, such as convoluted neural network and occupancy networks may prove to be a viable method for efficient simultaneous VWC and EC estimations, and it should be another topic for future investigations.

Declaration

(1) The authors declare that they have no known competing financial interests or personal relationships that could have appeared to influence the work reported in this paper.
(2) This paper does not constitute a standard, specification, regulation, or recommendation for the TDR construction, measurement, data analysis.
(3) The computer program mentioned in the manuscript is available at (https://github.com/cauwzj).

CRediT authorship contribution statement

Zhuangji Wang: Conceptualization, Formal analysis, Methodology, Software, Writing - original draft. **Dennis Timlin:** Conceptualization, Methodology, Writing - review & editing, Supervision. **Yuki Kojima:** Data curation, Methodology, Writing - review & editing. **Chenyi Luo:** Data curation, Writing - review & editing. **Yan Chen:** Conceptualization, Writing - review & editing, Supervision. **Sanai Li:** Methodology, Software, Writing - review & editing. **David Fleisher:** Conceptualization, Supervision, Writing - review & editing. **Katherine Tully:** Conceptualization, Supervision, Writing - review & editing. **Vangimalla R. Reddy:** Conceptualization, Supervision, Writing - review & editing. **Robert Horton:** Conceptualization, Methodology, Writing - review & editing, Supervision.

Declaration of Competing Interest

The authors declare that they have no known competing financial interests or personal relationships that could have appeared to influence the work reported in this paper.

Acknowledgements

This material is based upon work supported by the Department of Agriculture, Agricultural Research Service under Agreement No. 58-8042-7-067, National Science Foundation under Grant 1623806, and USDA-NIFA Multi-State Project 4188. The authors also received support from the University of Maryland and Iowa State University.

References

Adewumi, A.O., Akindeinde, S.O., Aderogba, A.A., Ogundare, B.S., 2017. Laplace transform collocation method for solving hyperbolic telegraph equation. Int. J. Eng. Math. https://doi.org/10.1155/2017/3504962.
Agah, A.E., Meire, P., de Deckere, E., 2019. Laboratory calibration of TDR probes for simultaneous of measurements soil water content and electrical conductivity. Commun. Soil Sci. Plan. 50, 1525–1540. https://doi.org/10.1080/00103624.2019.1626869.
Ankeny, M.D., Kaspar, T.C., Horton, R., 1988. Design for an automated tension infiltrometer. Soil Sci. Soc. Am. J. 52, 893–896. https://doi.org/10.2136/sssaj1988.03615995005200030054x.
Chen, Y., Wang, Z., Zhang, K., 2013. Approximations for modulus of gradients and their applications to neighborhood filters. Front. Math. China 8, 761–782. https://doi.org/10.1007/s11464-013-0297-7.
Coppola, A., Smettem, K., Ajeel, A., Saeed, A., Dragonetti, G., Comegna, A., Lamaddalena, N., Vacca, A., 2016. Calibration of an electromagnetic induction sensor with time-domain reflectometry data to monitor rootzone electrical conductivity under saline water irrigation. Eur. J. Soil Sci. 67, 737–748. https://doi.org/10.1111/ejss.12390.
Corwin, D.L., Lesch, S.M., 2005. Apparent soil electrical conductivity measurements in agriculture. Comput. Electron. Agric. 46, 11–43. https://doi.org/10.1016/j.compag.2004.10.005.
Dalton, F.N., Herkelrath, W.N., Rawlins, D.S., Rhoades, J.D., 1984. Time domain reflectometry: simultaneous in-situ measurement of soil water content and electrical conductivity with a single probe. Science 224, 989–990. https://doi.org/10.1126/science.224.4652.989.
Gaur, A., Jaynes, D.B., Horton, R., Ochsner, T.E., 2007. Surface and subsurface solute transport properties at row and inter-row positions. Soil Sci. 172, 419–431. https://doi.org/10.1097/ss.0b013e3180471c72.
Giese, K., Tiemann, R., 1975. Determination of the complex permittivity from thin-sample 372 time domain reflectometry improved analysis of the step waveform. Adv. Mol. Relax. 373 Processes 7, 45–59. doi: 10.1016/0001-8716(75)80013-7.
Greco, R., 2006. Soil water content inverse profiling from single TDR waveforms. J. Hydrol. 317, 325–339. https://doi.org/10.1016/j.jhydrol.2005.05.024.
Griffin, G.P., Jurinak, J.J., 1973. Estimation of activity coefficients from the electrical conductivity of natural aquatic systems and soil extracts. Soil Sci. 116, 26–30.
Heimovaara, T.J., 1994. Frequency domain analysis of time domain reflectometry waveforms, 1, Measurement of the complex dielectric permittivity of soils. Water Resour. Res. 30, 189–199. https://doi.org/10.1029/93WR02948.

Heitman, J.L., Gaur, A., Horton, R., Jaynes, D.B., Kaspar, T.C., 2007. Field measurement of soil surface chemical transport properties for comparison of management zones. Soil Sci. Soc. Am. J. 71, 529–536. https://doi.org/10.2136/sssaj2006.0254.

Lin, C.P., Chung, C.C., Huisman, J.A., Tang, S.H., 2008. Clarification and calibration of reflection coefficient for electrical conductivity measurement by time domain reflectometry. Soil Sci. Soc. Am. J. 72, 1033–1040. https://doi.org/10.2136/sssaj2007.0185.

Lu, Y., Liu, X., Zhang, M., Heitman, J., Horton, R., Ren, T., 2017. Thermo–time domain reflectometry method: advances in monitoring in situ soil bulk density. Methods Soil Anal. 2 https://doi.org/10.2136/msa2015.0031.

Luo, C., Wang, Z., Kordbacheh, F., Li, S., Cetin, B., Ceylan, H., Horton, R., 2020. A greenhouse study of concrete grinding residue influences on seedling emergence and early growth of selected prairie species. Water Air Soil Pollut. 231, 253. https://doi.org/10.1007/s11270-020-04580-4.

Mazurek, P., Putynkowski, G., 2016. Frequency management for electromagnetic continuous wave conductivity meters. Sensors. 16, 490. https://doi.org/10.3390/s16040490.

Minet, J., Lambot, S., Delaide, G., Huisman, J.A., Vereecken, H., Vanclooster, M., 2010. A generalized frequency domain reflectometry modeling technique for soil electrical properties determination. Vadose Zone J. 9, 1063–1072. https://doi.org/10.2136/vzj2010.0004.

Mirzakhaninafchi, H., Mani, I., Nafchi, A.M., 2017. Study on Soil nitrogen and electrical conductivity relationship for site-specific nitrogen application. ASABE Ann. Int. Meet. https://doi.org/10.13031/aim.201700892.

Munoz-Carpena, R., Regalado, C.M., Ritter, A., Alvarez-Benedi, J., Socorro, A.R., 2005. TDR estimation of electrical conductivity and saline solute concentration in a volcanic soil. Geoderma 124, 399–413. https://doi.org/10.1016/j.geoderma.2004.06.002.

Nadler, A., Dasberg, S., Lapid, I., 1991. Time domain reflectometry measurements of water content and electrical conductivity of layered soil columns. Soil Sci. Soc. Am. J. 55, 938–943. https://doi.org/10.2136/sssaj1991.03615995005500040007.

Noborio, K., 2001. Measurement of soil water content and electrical conductivity by time domain reflectometry: a review. Comput. Electron. Agric. 31, 213–237. https://doi.org/10.1016/S0168-1699(00)00184-8.

Ochiai, H., Noborio, K., Mizoguchi, M., 2010. Evaluating average electrical conductivity of a layered soil measured with a vertically-installed time domain reflectometry probe. J. Jpn. Soc. Soil Phys. 116, 3–8 (in Japanese with English abstract).

Oswald, B., Benedickter, H.R., Bauchtold, W., Flühler, H., 2003. Spatially resolved water content profiles from inverted time domain reflectometry signals. Water Resour. Res. 39, 1357. https://doi.org/10.1029/2002WR001890.

Peng, W., Lu, Y., Xie, X., Ren, T., Horton, R., 2019a. An improved thermo-TDR technique for monitoring soil thermal properties, water content, bulk density, and porosity. Vadose Zone J. 18, 1–9. https://doi.org/10.2136/vzj2019.03.0026.

Peng, Y., Xiao, Y., Fu, Z., Dong, Y., Zheng, Y., Yan, H., Li, X., 2019b. Precision irrigation perspectives on the sustainable water-saving of field crop production in China: water demand prediction and irrigation scheme optimization. J. Clean. Prod. 230, 365–377. https://doi.org/10.1016/j.jclepro.2019.04.347.

Raftari, B., Yildirim, A., 2010. Analytical solution of second-order hyperbolic telegraph equation by variational iteration and homotopy perturbation methods. Results. Math. 61, 13–28. https://doi.org/10.1007/s00025-010-0072-y.

Ramo, S., Whinnery, J.R., van Duzer, T., 1984. Fields and Waves in Communication Electronics, 2nd ed. John Wiley, Hoboken, N.J.

Rashidinia, J., Jamalzadeh, S., Esfahani, F., 2014. Numerical solution of one-dimensional telegraph equation using cubic B-spline collocation method. J. Interpol. Approx. Sci. Comput. 2014, 1–8. https://doi.org/10.5899/2014/jiasc-00042.

Requena-Pérez, M.E., Albero-Ortiz, A., Monzó-Cabrera, J., Díaz-Morcillo, A., 2006. Combined use of genetic algorithms and gradient descent optimization methods for accurate inverse permittivity measurement. IEEE T. Microw. Theory. 52, 615–624. https://doi.org/10.1109/TMTT.2005.862671.

Robinson, D.A., Jones, S.B., Wraith, J.M., Or, D., Friedman, S.P., 2003. A review of advances in dielectric and electrical conductivity measurement in soils using time domain reflectometry. Vadose Zone J. 2, 444–475. https://doi.org/10.2136/vzj2003.4440.

Sanches, G.M., Magalhães, P.S.G., Remacre, A.Z., Franco, H.C.J., 2018. Potential of apparent soil electrical conductivity to describe the soil pH and improve lime application in a clayey soil. Soil Till. Res. 175, 217–225. https://doi.org/10.1016/j.still.2017.09.010.

Schwartz, R.C., Casanova, J.J., Bell, J.M., Evett, S.R., 2013. A reevaluation of time domain reflectometry propagation time determination in soils. Vadose Zone J. 13 (1) https://doi.org/10.2136/vzj2013.07.0135.

Sheng, W., Zhou, R., Sadeghi, M., Babaeian, E., Robinson, D.A., Tuller, M., Jones, S.B., 2017. A TDR array probe for monitoring near-surface soil moisture distribution. Vadose Zone J. 16 https://doi.org/10.2136/vzj2016.11.0112.

Shuai, X., Green, T.R., Logsdon, S., 2017. Improved theory of time domain reflectometry with variable coaxial cable length for electrical conductivity measurements. Soil Sci. Soc. Am. J. 81, 723–733. https://doi.org/10.2136/sssaj2016.09.0297.

Tian, Z., Kojima, Y., Heitman, J., Horton, R., Ren, T., 2018. Advances in thermo-time domain reflectometry technique: measuring ice content in partially frozen soils. Methods Soil Anal. 4, 1. https://doi.org/10.2136/msa2019.0003.

Timlin, D.J., Pachepsky, Y.A., 1996. Comparison of three methods to obtain the apparent dielectric constant from time domain reflectometry wave traces. Soil Sci. Soc. Am. J. 60, 970–977.

Timlin, D.J., Pachepsky, Y.A., 2002. Infiltration measurement using a vertical time-domain reflectometry probe and a reflection simulation model. Soil Sci. 167, 1–8.

Todoroff, P., Lorion, R., Lan Sun Luk, J.D., 1998. L'utilisation des algorithms génétiques pour l'identification de profils hydriques de sol à partir de courbes réflectométriques. C. R. Acad. Sci. Ser. II. Sci. Terre Planetes. 327, 607–610.

Topp, G.C., Davis, J.L., Annan, A.P., 1980. Electromagnetic determination of soil water content: measurement in coaxial transmission lines. Water Resour. Res. 16, 574–582. https://doi.org/10.1029/WR016i003p00574.

Topp, G.C., Yanuka, M., Zebchuk, W.D., Zegelin, S., 1988. Determination of electrical conductivity using time domain reflectometry: soil and water experiments in coaxial lines. Water Resour. Res. 24, 945–952. https://doi.org/10.1029/WR024i007p00945.

Wang, Z., Kojima, Y., Lu, S., Chen, Y., Horton, R., Schwartz, R.C., 2014. Time domain reflectometry waveform analysis with second-order bounded mean oscillation. Soil Sci. Soc. Am. J. 78, 1146–1152. https://doi.org/10.2136/sssaj2013.11.0497.

Wang, Z., Lu, Y., Kojima, Y., Lu, S., Zhang, M., Chen, Y., Horton, R., 2016. Tangent line/second-order bounded mean oscillation waveform analysis for short TDR probe. Vadose Zone J. 15 (1) https://doi.org/10.2136/vzj2015.04.0054.

Wang, Z., Schwartz, R.C., Kojima, Y., Chen, Y., Horton, R., 2017. A comparison of second-order derivative based models for time domain reflectometry waveform analysis. Vadose Zone J. 16 (7) https://doi.org/10.2136/vzj2017.01.0014.

Yang, B., Cetin, B., Zhang, Y., Luo, C., Ceylan, H., Horton, R., Kim, S., Mahedi, M., 2019. Effects of concrete grinding residue (CGR) on selected sandy loam properties. J. Clean Prod. 240, 118057 https://doi.org/10.1016/j.jclepro.2019.118057.

Yanuka, M., Topp, G.C., Zegelin, S., Zebchuk, W.D., 1988. Multiple reflection and attenuation of time domain reflectometry pulses: theoretical considerations for applications to soil and water. Water Resour. Res. 24, 939–944. https://doi.org/10.1029/WR024i007p00939.